European Journal of Medicinal Chemistry 46 (2011) 3265–3273

Contents lists available at ScienceDirect

European Journal of Medicinal Chemistry

journal homepage: http://www.elsevier.com/locate/ejmech

Original article

Antiproliferative activity of aroylacrylic acids. Structure-activity study based on molecular interaction fields

Branko J. Drakulić [a,*], Tatjana P. Stanojković [b], Željko S. Žižak [b], Milan M. Dabović [a]

[a] Department of Chemistry-Institue of Chemistry, Technology and Metallurgy, University of Belgrade, Njegoševa 12, 11000 Belgrade, Serbia
[b] Institute of Oncology and Radiology of Serbia, Pasterova 14, 11000 Belgrade, Serbia

ARTICLE INFO

Article history:
Received 14 February 2011
Received in revised form
9 April 2011
Accepted 13 April 2011
Available online 21 April 2011

Keywords:
4-aryl-4-oxo-2-butenoic acids
Antiproliferative activity
Human tumors
Molecular interaction fields

ABSTRACT

Antiproliferative activity of 27 phenyl-substituted 4-aryl-4-oxo-2-butenoic acids (aroylacrylic acids) toward Human cervix carcinoma (HeLa), Human chronic myelogenous leukemia (K562) and Human colon tumor (LS174) cell lines *in vitro* are reported. Compounds are active toward all examined cell lines. The most active compounds bear two or three branched alkyl or cycloalkyl substituents on phenyl moiety having potencies in low micromolar ranges. One of most potent derivatives arrests the cell cycle at S phase in HeLa cells. The 3D QSAR study, using molecular interaction fields (MIF) and derived alignment independent descriptors (GRIND-2), rationalize the structural characteristics correlated with potency of compounds. Covalent chemistry, most possibly involved in the mode of action of reported compounds, was quantitatively accounted using frontier molecular orbitals. Pharmacophoric pattern of most potent compounds are used as a template for virtual screening, to find similar ones in database of compounds screened against DTP-NCI 60 tumor cell lines. Potency of obtained hits is well predicted.

1. Introduction

First synthesis of parent 4-phenyl-4-oxo-2-butenoic acid (**1**, benzoylacrylic acid) has been reported 1882 [1]. Since then number of congeners was synthesized, and they're antibacterial activity and 2D QSAR was described [2]. It was shown that ketovinyl part of molecule (−C(O)−C═C−) acts as Michel acceptor that covalently bind reactive sulfhydryl (−SH) groups of biomolecules [3]. Cytembena, 4-(4-methoxyphenyl)-4-oxo-3-bromo-butenoic acid (NSC 104801), structurally similar to aroylacrylic acids have been extensively studied during late sixteen's of the last century as cytostatic agent [4], and was discontinued for further usage due to sever side-effects. In previous article [5] we have reported antiproliferative activity of nineteen aroylacrylic acids (**1**–**6**, **8**–**11**, **14**, **20**–**26** as given in Table 1, and 4−$CH_3C(O)NH$- phenyl substituted derivative) toward human cervix carcinoma cells (HeLa), after 42 h of exposure to compounds. The 2D QSAR study shown that potency of compounds is well correlated with estimated lipophilicity. Even Michael acceptor comprising molecules are commonly flagged as less than optimal leads, due to its potential promiscuity and consequent toxicity, accumulated examples, reported recently [6], of using ketovinyl moiety as a warhead for directed and selective covalent inhibition of diverse pharmacological targets trigger our interest to further evaluate previous findings. Recently reported suicide inhibitor [7] that selectively target proteosome of HIV infected cells, bear ketovinyl moiety as covalent warhead. Covalent inhibitors of epidermal growth factor receptor (EGFR), as Neratinib [8] and Pelitinib [9], incorporates ketovinyl moiety that target conserved cystein residue in the ATP binding site, overcoming in this way resistance to previous generation of non-covalent inhibitors. Along with this, integrated bioinformatic analysis of National Cancer Institute inhibition profile for the database [10] of compounds screened across a panel of tumor cells (NCI60) [11] as possible targets for ketovinyl containing compounds propose gluthathione *S*-transferase, acting in cellular detoxification, as well as NFκB (nuclear factor kappa-light-chain-enhancer of activated B cells) involved in cellular response to stress. It should be noted that number of chalcones and derivatives (suberones and similar), structurally related to 4-aryl-4-oxo-2-butenoic acids, exert significant antiproliferative potency. Majority of compounds within this class bear HBD/HBA, or polar substituents on phenyl rings (MeO−, OH−, $-NO_2$, $-OCH_2O-$, or halogen) [12]. Within our set, alkyl substituted compounds are most potent.

2. Results and discussion

In this article we report the synthesis, antiprolferative activity of twenty-seven (*E*)-4-aryl-4-oxo-2-butenoic acid (**1**–**27**) toward

* Corresponding author. Tel.: +381 113336738; fax: +381 112636061.
E-mail address: bdrakuli@chem.bg.ac.rs (B.J. Drakulić).

0223-5234/$ – see front matter © 2011 Elsevier Masson SAS. All rights reserved.
doi:10.1016/j.ejmech.2011.04.043

Table 1
Structures and IC_{50} (μM) values of antiproliferative potency for compounds **1**–**27**, determined under exactly same conditions.

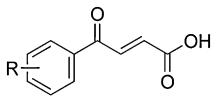

Compound No	R-	IC_{50} (μM)[a]		
		HeLa	LS174	K562
1	H-	30.64 (±4.14)	45.53 (±6.59)	30.19 (±0.77)
2	4-Me-	7.62 (±3.08)	28.42 (±2.32)	9.17 (±2.40)
3	4-Et-	27.79 (±3.25)	21.04 (±4.91)	5.53 (±0.95)
4	4-*i*-Pr-	4.90 (±1.32)	25.65 (±2.55)	5.56 (±0.53)
5	4-*n*-Bu-	4.78 (±1.45)	6.74 (±2.00)	4.95 (±0.59)
6	4-*tert*-Bu-	5.10 (±0.82)	8.74 (±1.57)	4.33 (±0.45)
7	4-*n*-dodecyl-	5.82 (±0.66)	7.85 (±1.15)	4.01 (±0.56)
8	2,4-di-Me-	6.06 (±1.18)	7.08 (±2.30)	5.35 (±0.29)
9	2,5-di-Me-	7.86 (±0.84)	21.98 (±1.90)	5.90 (±0.28)
10	3,4-di-Me-	7.28 (±1.37)	12.11 (±5.74)	5.62 (±0.49)
11	β-tetralinyl-	7.01 (±0.90)	17.58 (±2.59)	5.60 (±0.51)
12	2-Et-5-*i*-Pr-	4.89 (±0.46)	5.94 (0.594)	1.36 (±0.59)
13	2,4-di-*i*-Pr-	4.06 (±0.97)	5.36 (±0.56)	4.68 (±1.61)
14	2,5-di-*i*-Pr-	4.75 (±0.51)	6.23 (±0.33)	3.28 (±1.18)
15	2,4,6-tri-Et-	6.53 (±1.55)	7.28 (±1.77)	4.01 (±0.89)
16	2,4,6-tri-*i*-Pr-	6.10 (±1.40)	8.28 (±1.54)	4.67 (±0.09)
17	2-Et-3,5-di-*i*-Pr-	7.61 (±1.87)	12.35 (±4.88)	5.10 (±0.14)
18	4-Ch-2,5-di-Me-	2.38 (±0.65)	6.64 (±1.20)	4.24 (±0.23)
19	2,5-di-Ch-	1.26 (±0.02)	4.28 (±0.60)	3.32 (±0.63)
20	2-Cl-4-Me-	7.60 (±1.73)	27.69 (±6.99)	14.59 (±6.52)
21	4-F-	28.41 (±5.29)	33.78 (±3.37)	16.90 (±5.12)
22	4-Cl-	25.42 (±2.43)	28.65 (±6.12)	21.66 (±4.36)
23	4-Br-	18.68 (±4.20)	27.12 (±4.14)	11.19 (±2.15)
24	2,4-di-Cl-	62.94 (±5.50)	>100	58.47 (±12.23)
25	3,4-di-Cl-	28.30 (±3.66)	32.33 (±3.65)	23.15 (±9.67)
26	4-MeO-	27.36 (±7.15)	34.74 (±11.41)	12.32 (±9.21)
27	2,3,4-tri-MeO-	96.18 (±2.16)	> 100	> 100

[a] Mean of three measurements, each performed in triplicate.

three human tumor cell lines, and 3D QSAR, aimed to rationalize structural characteristics needed for significant potency. Compounds were obtained by Friedel-Crafts acylation of aromatic substrates with maleic acid anhydride in good yields (Scheme 1).

Structures of compounds **1**–**27** are given in Table 1. Even known from literature data, stereochemistry on ketovinyl double bond is proved by single crystal x-ray structure data for compound **1** [13], and **13** [14] (Figure S1 in Supplementary material), as well as from the coupling constants of (keto)vinyl protons in ^{1}H NMR spectra for all derivatives. Vinyl protons of derivatives having *E*-stereochemistry show coupling constants of ~16 Hz [15].

Antiproliferative activity of compounds was assessed toward Human cervix carcinoma (HeLa), Human chronic myelogenous leukemia (K562) and Human colon tumor (LS174) cell lines *in vitro*. The majority of compounds exert potency toward all tested cell lines in two-digit to low micromolar concentrations (Table 1).

Brief structure-activity for potency of **1**–**27** is as follows: Halogen- and methoxy- substituted compounds are less potent than alkyl-substituted congeners. Within group of alkyl-substituted compounds, those having two, or three branched alkyl (or cycloalkyl, as in **18** and **19**) substituents are more potent than the rest. It should be noted that increases in the number of alkyl substituents did not progressively contribute to potency. Overall, within the subset of most potent compounds (**12**–**19**), those having two substituents are more potent than the rest having three substituents, and most potent compounds have substituents in positions **2** and **5**.

According to *in vivo* tests, reported by NCI-DTP, compound **9** (NSC 329366) is well tolerated in P388 Leukemia model in CD2F1 (CDF1) mice, by intraperitoneal administration, in concentration up to 50 mg/kg; while compound **1** (NSC 143) is well tolerated in L1210 Leukemia model in CD2F1 (CDF1) mice by intraperitoneal administration in concentration up to 25 mg/kg.[1]

Cell cycle on HeLa cells was monitored after 24 h, 48 h and 72 h treatment of cells with compound **19**. Results are given in Fig. 1 and Table S1 in Supplementary material. Compound **19** arrests the cell cycle at S phase, as can be seen from data obtained after 24 and 48 h. After 72 h, compound caused extensive damage of cells, as can be seen from high subG1 band in (Fig. 1c). It is known that resistance and sensitivity of cells toward radiation correlates with the level of sulfhydryl compounds in the cell. Nonprotein sulfhydryls (NPS), are natural radioprotector, as well as powerful antioxidative protector, and tend to be at highest level in S phase of the cell cycle. Because of that cells exert lowest sensitivity to radiation in this phase. Ketovinyl containing compounds are powerful thiol "quenchers", so this fact is often used as possible explanation for the potency of such compounds toward malignant cells; ketovinyl containing compounds bind NPS, and make cells more sensitive to oxidative stress [16]. Even such scenario coincide with our results, in the light of knowledge of protein targets, spanning the range from long time known gluthathione *S*-transferase to widespread kinases in last decades, which are prompt to covalent inhibition by ketovinyl derivatives, we can speculate that quenching of NPS can only partially explain the mode of action of our compounds.

To obtain deeper insight in structural features that govern differences in potency, we performed 3D quantitative structure-activity relationships (3D QSAR). For the 3D QSAR, molecular interaction fields (MIF) obtained by GRID programme were calculated using hydrogen bond acceptor (carbonyl oxygen O), hydrogen bond donor (neutral flat amine, N1), hydrophobic (DRY), and shape (TIP) [17] probes. Alignment independent descriptors (GRIND-2) [18], derived from obtained MIF, are subsequently processed by partial least square analysis (PLS), as applied in Pentacle software [19], for details see experimental part.

All obtained models have a good statistics (Table 2). In PCA models, five principal components explain 56–60% variance (Table S2 in Supplementary material). Antiproliferative potency of **1**–**27** toward HeLa and LS174 cell lines were explained by 3 latent variables (LV) models. For the action of compounds toward K562, 4LV model was used.

Three LV PLS coefficient plots for potency of compounds toward HeLa and LS174 cells are given on Figs. 2a and 2b. Four LV PLS coefficient plot for potency of compounds toward K562 cells is given on (Fig. 2c). Associations of variables with compounds are given in Tables S3–5 in Supplementary material. Experimental *vs.* calculated p(IC_{50}) values are given in Table S6 in Supplementary material.

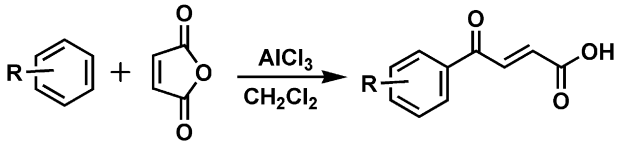

Scheme 1. Syntheses of **1**–**27**, R is as given in Table 1.

[1] In NCI-DTP database (http://dtp.nci.nih.gov/dtpstandard/dwindex/index.jsp) compounds **1** (NSC 143), **7** (NSC 30659), **8** (NSC 31589), **9** (NSC 329366), **22** (NSC 32875), **23** (NSC 39971), and **26** (NSC 25331) were recorded. NCI60 cell line screening data were not performed for those compounds. Only yeast screening data, and *in vivo* screening data for **1** and **9** exists.

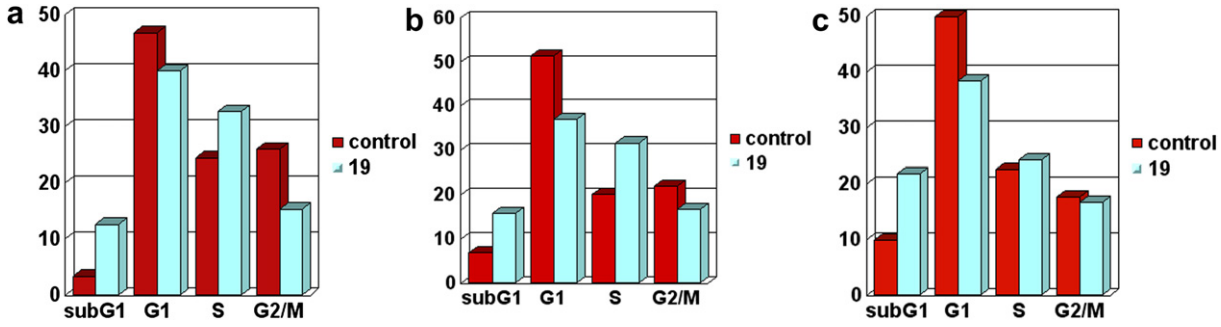

Fig. 1. Effect of **19** on cell cycle distribution in HeLa cells, after a) 24 h, b) 48 h, and c) 72 h treatment of cells with compound.

As can be seen from Table 1, the order of potency of **1**–**27** toward tested cell lines are similar, but not the same, so appearance of common variables having high positive or negative impact on models, within all three PLS coefficient plots, are briefly outlined to explain how structural variation govern differences of potency among compounds.

- Compounds most potent toward all cell lines tested have branched alkyl substituents in positions **2** and **5** of the phenyl ring. Variables DRY-DRY 36, 37 and 39, for K562, LS174, and HeLa model, respectively, positively correlated with the potency, even haven't highest impact on overall models, nicely distinguishes most potent compounds from less potent ones. Those variables connect nodes of the DRY field interacting with the ketovinyl –C═C–, and with the 5 alkyl (or cycloalkyl) substituent (spatial distance of DRY nodes are 11.50–12.80 Å), as illustrated on Fig. 3a, for compound **13**, HeLa model.
- Variable TIP-TIP 311 in K562 and HeLa model, is expressed for all compounds, except for 4-*n*-dodecyl derivative (**7**), distinguishing in this way compound that have a significantly longer 4-alkyl substituent.
- Variables TIP-TIP 319 and 320, for K562 and HeLa model, respectively, negatively correlated with potency are expressed for majority of compounds having 4-alkyl substituent. This emphasize that 2,5-di-alkyl substituted compounds are more potent than those that bear substituent in position 4, yet this is bulky alkyl substituent. Variable connect nodes of TYP probe on distance 16.00–17.28 Å, associated with the carboxyl group and with the bulkier substituent in position 3- or 4- of the phenyl ring, as is illustrated on Fig. 3b for compound **18**, K562 model.
- In HeLa model, variable DRY-O 403, positively correlated with potency, gives almost clear-cut between more potent alkyl

Table 2
3LV PLS models for the potency of compounds toward HeLa and LS174 cells, and 4LV PLS models for the potency of compounds toward K562 cells.

Component	SSX	SSX_a	SDEC	SDEP	R^2	R^2_{acc}	Q^2_{acc}	LOO	Q^2_{acc}	LTO	Q^2_{acc}	RG
HeLa PLS model												
1	23.95	23.95	0.27	0.34	0.61	0.61	0.41		0.41		0.39	
2	25.58	49.53	0.18	0.29	0.22	0.83	0.56		0.56		0.54	
3	8.12	57.65	0.13	0.28	0.08	0.91	0.61		0.61		0.59	
LS174 PLS model												
1	29.80	29.80	0.20	0.23	0.59	0.59	0.53		0.52		0.49	
2	27.66	57.46	0.13	0.18	0.23	0.82	0.68		0.68		0.68	
3	8.07	65.53	0.10	0.18	0.08	0.90	0.66		0.66		0.67	
K562 PLS model												
1	30.34	30.34	0.25	0.29	0.48	0.48	0.36		0.36		0.31	
2	22.17	52.51	0.17	0.24	0.27	0.74	0.53		0.52		0.51	
3	7.11	59.62	0.13	0.24	0.12	0.86	0.56		0.55		0.51	
4	4.03	63.66	0.08	0.24	0.08	0.95	0.55		0.55		0.52	

SSX - Percentage of the X sum of squares; SSX_{acc} - accumulative percentage of the X sum of squares; SDEP - standard deviation of error of the predictions; R^2 - coefficient of determination; R^2_{acc} - accumulative coefficient of determination; Q^2_{acc} - accumulative squared predictive correlation coefficient; LOO - leave one out, LTO - leave two out; RG - random groups (three random group of approximately same size were used).

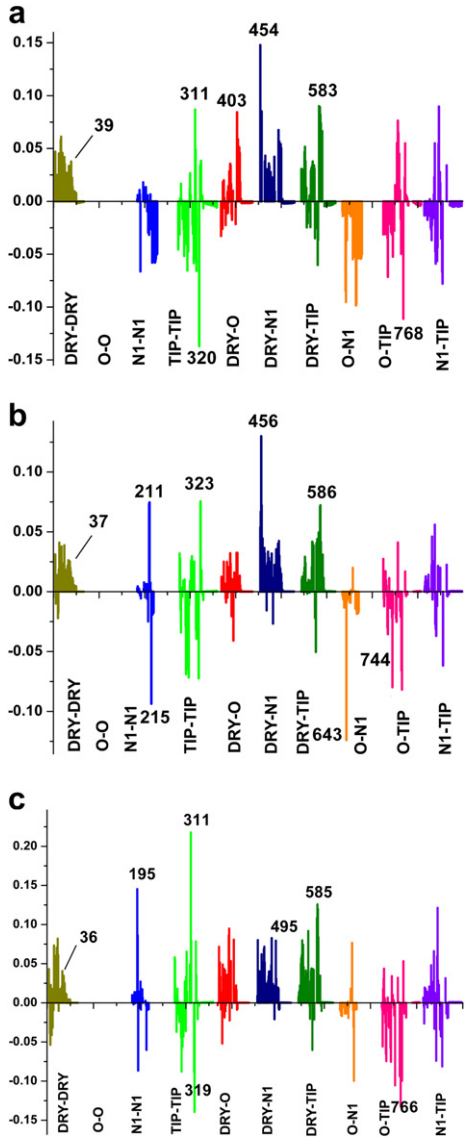

Fig. 2. 3LV PLS coefficient plots for the model for potency of compounds toward HeLa a), and LS174 b) cells, and 4LV PLS coefficient plots for the model for potency compounds toward K562 cells, c).

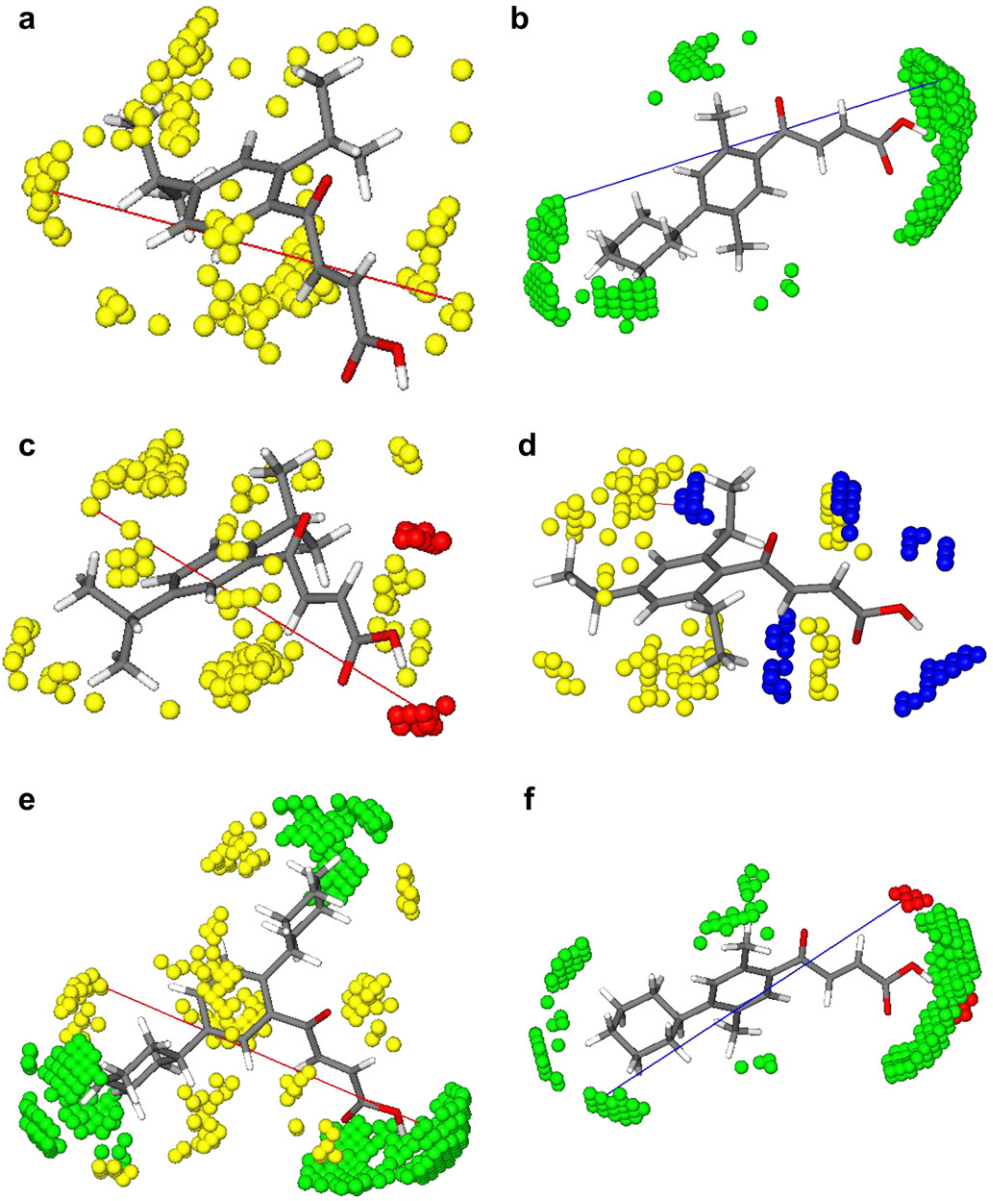

Fig. 3. Examples of variables associated with compounds, as described in the text. a) Variable DRY-DRY 39 for compound **13**, HeLa model. b) Variable TIP-TIP 320 for compound **18**, K562 model. c) Variable DRY-O 403 for compound **14**, HeLa model. d) Variable DRY-N1 454 for compound **15**, HeLa model. e) Variable DRY-TIP 586 for compound **19**, LS174 model. f) Variable O-TIP 768 for compound **18**, HeLa model.

substituted compounds, bearing bulkier substituents, from other, less potent. Node of O probe is always associated with carboxyl –OH, while DRY probe nodes, on distance 13.76–14.08 Å, are associated with *meta* or *para* substituents. This is illustrated on Fig. 3c, for compound **14**, HeLa model. In K562 model similar variable, DRY-O 404, appear.

- Variable DRY-N1 454, and 459, for HeLa and LS174 models, respectively, has highest positive impact on model. Variable connect nodes of the hydrophobic DRY probe above phenyl ring and nodes of hydrogen bond donor probe (N1) interacting with aroyl oxygen, on short distance of 1.28–2.24 Å, as is illustrated on Fig. 3d, for compound **15**, HeLa model. Variable is expressed for most potent compounds, that have bulky alkyl substituents in *ortho* position. Such substituents cause significant torsion between phenyl moiety and aroyl keto group. Similarly, long time ago in literature have been emphasized that aroylacrylic acids and derivatives bearing *ortho* alkyl substituents are more potent antibacterial agents than those which have different substitution pattern on the phenyl ring [2b].
- Next variables positively correlated with potency, in all models, are DRY-TIP 583, 585 and 586 for HeLa, K562 and LS174 models, respectively. Those variables well separate more potent compounds from less potent ones. TIP node is associated with –COOH group, common for all compounds, while DRY nodes, on distance 13.76–15.04 Å, are associated with bulkier substituents in positions 2, 3 or 4. This is illustrated on Fig. 3e, for compound **19**, LS174 model.
- Variables O-TIP 766 and 768, for K562 and HeLa models, respectively, negatively correlated with potency, similar as TIP-TIP 320, in majority are not expressed for compounds having unsubstituted position 4. Variable is illustrated on Fig. 3f, for compound **18**, HeLa model. In HeLa model variable O-TIP 766 distinguish 2,5-disubstituted derivatives having medium-size alkyl substituents (**9** and **12**) from the rest of

compounds. O node is associated with –COOH group, while TIP nodes, at distance 14.40–15.36 Å, are associated with substituents in positions 3- or 4-.

Other variables having significant impact on models (those having significant positive or negative intensity on Fig. 2a, b and c, but not assigned by numbers) were not commented, because those variables are expressed for all compounds, or only distinguish compound **7** from the rest, as is exemplified with the variable TIP-TIP 311 in K562 and HeLa model.

In the next step we try to find out whether 3D-dependent whole molecular descriptors show correlation with the potency of compounds. Therefore, we calculated virtual log*P* [20], molecular surfaces (solvent accessible, polar, apolar), volume, as well as isosurfaces obtained by GRID DRY, OH2 and H probe on visually chosen isoenergetic values (Table S7 in Supplementary material). The best correlation for potency of compounds toward all three cell lines are obtained between p(IC_{50}) values and ratio of apolar to total surface area (r = 0.74 (HeLa), 0.77 (K562); 0.86 (LS174)). Other linear correlations that include up to 3 descriptors (MLR), yield significantly inferior statistical results.

We speculate that our compounds exert biological activity by Michael-type addition of thiol and amino group of enzymes amino acid side chains. On the ground of literature data and experiments performed in our laboratory [21], aroylacrylic acids and derivatives make stable, non-reversible adducts with relatively simple thiols and amines, acting exclusively as unsaturated ketones, not as unsaturated acids. All descriptors described so far do not account for "covalent chemistry", most probably involved in the mode of biological action, so we extracted highest occupied molecular orbital (HOMO) and lowest unoccupied molecular orbital (LUMO) energies from MOPAC output files (Table S8 in Supplementary material), in attempt to include those data in our correlations. By using whole-molecular 3D descriptors (as described in previous paragraph), and HOMO and LUMO energies, fair, statistically significant correlations, that include ASA/SA ratio and energy of LUMO orbitals, appear for the potency of compounds toward HeLa and K562 cells:

$$p(IC_{50})_{HeLa} = -3.064(\pm 1.21)(ASA/SA) + 2.034(\pm 1.95)LUMO + 12.74(\pm 3.30) \quad (1)$$

($n = 27$; $r = 0.789$; $s = 0.282$; $F = 19.755$; $Q^2 = 0.529$; $s_{PRESS} = 0.315$)

Exclusion of compound **27** gives something better statistics ($r = 0.835$; $sd = 0.230$; $F = 26.537$; $Q^2 = 0.595$).

$$p(IC_{50})_{K562} = -2.509(\pm 0.89)(ASA/SA) + 1.727(\pm 1.44)LUMO + 11.56(\pm 2.45) \quad (2)$$

($n = 26$; $r = 0.825$; $s = 0.208$; $F = 24.560$; $Q^2 = 0.574$; $s_{PRESS} = 0.240$)

Exclusion of compounds **12** and **24** gives something better statistics ($r = 0.905$; $sd = 0.124$; $F = 47.291$; $Q^2 = 0.746$). For LS174 cells similar correlation could be obtained, but such correlation lack statistical significance.

Even ASA/SA term in Equations (1) and (2) lack in-dept structure-activity trends, as were obtained by Pentacle models (obvious that, within set of most potent **12**–**19**, molecules having two branched substituents exert better potency than those with three such substituents, so potency was not collinear with increase of the ratio between apolar and total surface area), it should be noted that both equations include LUMO energies, which are often associated with the susceptibility of molecules to nucleophilic attack. Along with this, for each molecule LUMO orbital is associated with ketovinyl moiety – target of nucleophilic attack in molecules, as is exemplified on Fig. 4 for compound **13**.

^{13}C Chemical shifts of the carbon atom 2 of butenoic moiety, that should be target of nucleophilic attack, or other carbons of ketovinyl moiety, extracted from HSQC spectra of most potent **12**–**19** did not show any correlation with potency data. This is not surprising because compounds act on whole cells, involving permeation in cell interior, reaching the potential intracellular target(s), and interaction with those targets. It should be noted that even on model system, introduction of *ortho* substituents in series of compounds structurally related to **1**–**27**, significantly deviate regularity of the change of electron density on carbon atom that act as a target for nucleophile attack, in respect to other compounds having para substituents, and for which good structure-activity relationship can be obtained using phenyl-substituents effect only [22]. Cited example describe variation of substituents bearing heteroatoms directly connected to phenyl ring, so having much stronger resonance effect than alkyl groups in our compounds.

In the next step we search NCI-DTP database for compounds active toward K562 cells that comprise ketovinyl moiety. Molecular mass of hits is limited to 400 (about 20% higher than mass of largest **19**), and chalcones and dibenzalacetones are excluded to preclude appearance of trivial results in virtual screening. Sixty-three compounds were collected in this way (Table S9 in Supplementary material), and database was made in Pentacle virtual screening (VS) mode, 19 principal components (PC) explain 85% of variance. Three compounds (**13**, **14** and **19**) were used as templates for VS. Database was "contaminated" with compound **14**, to test which method give best results for similarity search. Minimum distance was found as most suitable method, this is in accordance with data found in original article that describes Pentacle VS module [23]. To all PC's are ascribed same weights and VS were done with all 19 PC's. First three compounds that are identified as most similar to templates are: 1. NSC 145150 (CAS 70857-52-2, NCI 60 cell lines mean $pGI_{50} = 4.99$, K562 $pGI_{50} = 5.0$); 2. NSC 672120 (NCI 60 cell lines mean $pGI_{50} = 5.90$, K562 $pGI_{50} = 6.8$); and 3. NSC 321477 (CAS 28644-86-2, Zexbrevin, NCI 60 cell lines mean $pGI_{50} = 5.24$, K562 $pGI_{50} = 5.4$). Structures of these compounds are shown on Fig. 5.

All compounds are proved as active toward all NCI60 cell lines, Along with the antiproliferative activity, NSC 145150 is described as antibiotic [24]; while NSC 321477 is sesquiterpene lactone isolated from *Zexmenia brevifolia* and also exerts antibacterial and antifungal activity. As instant version of Pentacle does not offer visualization of variables most important for obtained similarity, we rebuilt whole model in Pentacle standard mode, to obtain **19** principal components PCA model. Such model explains same variance as in VS mode, so should be considered as valid. Compounds **13**, **14** and **19** were added to this set, and variables common to both NSC 145150, NSC

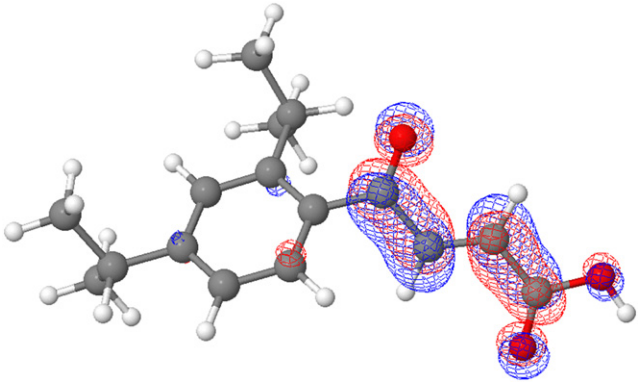

Fig. 4. The LUMO of compound **13**, –1.68 eV.

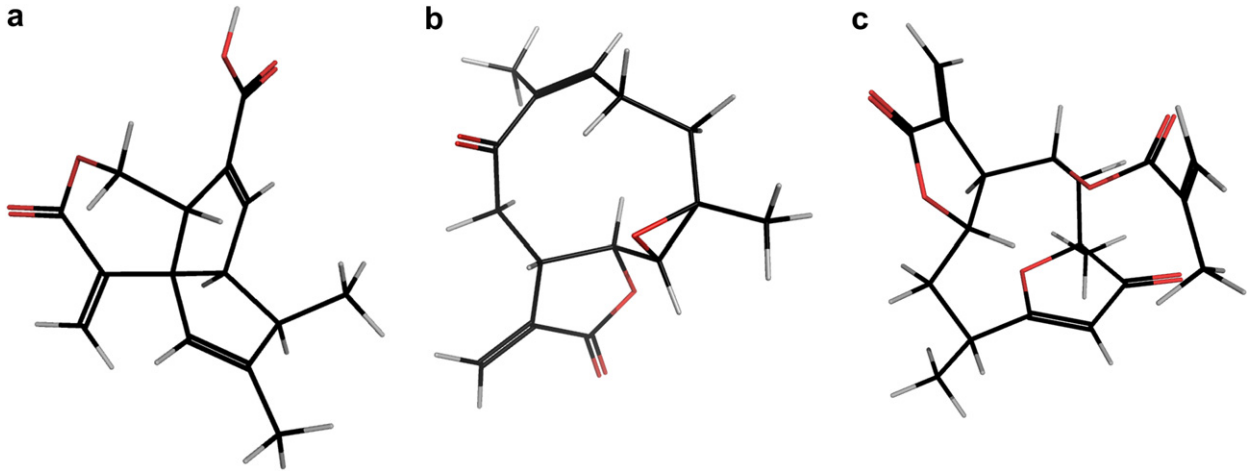

Fig. 5. Structures of a) NSC 145150, b) NSC 672120, and c) NSC 321477.

321477, NSC 672120, and **13**, **14** and **19** were found manually, searching regions of variables space near the variables which have highest impact on K562 model for **1**–**27**, as described above. In this way four variables, which reflects similarity among compounds, were chosen:[2] TIP-TIP covering distance 13.20–13.60 Å, illustrated on Figure S2a and b in Supplementary material, comparable with TIP-TIP 311 (13.12–13.44 Å); DRY-N1 covering distance 10.80–11.20 Å, illustrated on Figure S3a and b in Supplementary material, comparable with DRY-N1 495 (14.40–14.72 Å); DRY-TIP covering distance 11.20–11.60 Å, illustrated on Figure S4a and b in Supplementary material, comparable with DRY-TIP (14.40–14.72 Å); as well as DRY-DRY covering distance 4.80–5.20 Å, which cannot be found in models for potency of **1**–**27** toward studied cell lines, but nicely show fields associated with both activated double bond and proximal hydrophobic region of molecules, common to all molecules compared. This variable is illustrated on Figure S5a and b in Supplementary material. To illustrate similarity between MIF's of hits and template molecule, hot spots, as obtained by Pentacle, for **14**, NSC 145150, NSC 321477, and NSC 672120 are given in Supplementary as 3D files. Finally, we projected hits of our similarity search (NSC 145150, NSC 321477, NSC 672120) on the K562 model, using pGI_{50}[3] values to describe potency for NSC compounds. Good prediction were obtained with 4LV ($r^2 = 0.937$, SDEP = 0.05), for NSC 145150 (experimental 5.00, predicted 5.004), and NSC 321477 (experimental 5.40, predicted 5.33); while prediction failed for NSC 672120, for which pGI_{50} lay out of the potency range of **1**–**27**.

3. Conclusion

(*E*)-4-Aryl-4-oxo-2-butenoic acids exert antiproliferative activity against human malignant cells *in vitro*. Twenty-seven congeners tested toward Human cervix carcinma (HeLa), Human chronic myelogenous leukemia (K562) and Human colon tumor (LS174) cells are potent in two-digit micromolar to low micromolar concentrations. Representative compound arrests cell in the S phase of the cell cycle. Most potent compounds bear branched alkyl substituents in positions **2** and **5** of the phenyl ring. 3D structure-activity analysis rationalizes structural requirements for the significant potency. Simple MLR, that include LUMO energies indicate "covalent chemistry" involved in the mode of action of compounds, as is expected for ketovinyl containing derivatives. Similarity search performed by pharmacophore pattern comparison, using molecular interaction fields and derived GRIND-2 descriptors, identify similar compounds in NCI-DTP database, that contain ketovinyl moiety and exert potency toward K562 cells. The model obtained for **1**–**27** very well predicted potency of two of those compounds.

4. Experimental

4.1. Chemistry

All chemicals were purchased from Aldrich, Fluka or Merck, having >98% purity and were used as received. For synthesis of **1**–**27** the dry methylene-chloride was stored over molecular sieves. Separation of **12** was done on ICN 12–26, 60 Å silica gel, using two Büchi C-601 pumps supplied with C-615 pump manager. Melting points were determinate on Büchi apparatus in open capillary tubes and are uncorrected. The IR spectra are recorded on Thermo Nicollet 6700 FT-IR spectrophotometer (KBr pallet or ATR). ^1H and ^{13}C NMR spectra are recorded on Varian Gemini 200 spectrometer on 200/50 MHz, or Bruker AVANCE on 500/125 MHz in $CDCl_3$, or DMSO-d_6, using tetramethylsilane (TMS) as internal standard. HSQC (Heteronuclear Correlation spectra), of **12**–**19** were recorded on Bruker AVANCE spectrometer. All chemical shifts are reported in ppm downfield from TMS. The high-resolution mass spectra are recorded on Agilent 6200 LC/ESI-MS TOF instrument in methanol, with cone voltage of 70 V.

4.1.1. Synthesis

Compounds (**1**–**27**) are synthesized as described in literature [25], by Friedel-Crafts acylation of substituted benzenes with maleic acid anhydride using anhydrous $AlCl_3$ as the catalyst in dry CH_2Cl_2. The 6.125 g (62.5 mmol) of maleic acid anhydride, 16.5 g (125 mmol) of anhydrous $AlCl_3$ and 62.5 mmol of aromatic substrates were used. After 4–6 h of stirring on room temperature the reaction mixture was captured with ice/conc. HCl. The solvent was removed by steam distillation. The residuals was filtered on vacuum, or extracted by appropriate solvent. In this way obtained solids or oily substances are processed by solution of Na_2CO_3 to pH 8.5, filtered to remove traces of Al from catalyst, neutralized by dropwise addition of conc. HCl, filtered, than washed thoroughly by water, dried and crystallized from appropriate solvent. Yields of pure products were from 40 to 92%. The aromatic hydrocarbons for

[2] Please be aware that models for potency of **1**–**27** were made using grid resolution of 0.4 Å, while VS was done using grid resolution of 0.5 Å.

[3] NCI-DTP pGI_{50} was obtained after 48 h exposure of target cells to compounds, while pIC_{50} was obtained after 72 h exposure of target cells to compounds. For other differences see experimental, and http://dtp.nci.nih.gov/branches/btb/ivclsp.html.

synthesis of **12** and **17** were obtained as follows: Acylation of commercially available alkyl-substituted benzenes by acetyl chloride gives ketones that were purified by distillation under reduced pressure, and characterized by NMR spectroscopy. Pure ketones were reduced by Huang-Minlon procedure [26], purified by distillation, characterized by NMR spectroscopy and acylated as described above. Synthesis of **12** and **17** were started from 30 mmol of aromatic precursors. Compound **17** was isolated as a pure product. Compound **12** was obtained as the mixture of ~20% of 2-*i*-Pr-5-Et- derivative and ~80% 2-Et-5-*i*-Pr- derivative (estimated by the ratio under ^{1}H NMR signals) which is purified by medium pressure column chromatography using hexanes/AcOEt/AcOH 4: 1: 0.2 until 2-Et-5-*i*-Pr- derivative gives clear NMR spectra (~45% yield calculated on initial mixture). The minor derivative was discarded. 1,4-di-Me-2-cyclohexylbenzene was prepared according to described procedure [27], starting with 50 mmol of DCC. The pure product was isolated after vacuum distillation in 65% yield. Acylation, as described above gives pure **18**. Full characterization data of compounds (**1**–**27**) are given in Supplementary material.

4.2. Biological procedures

Stock solutions of **1**–**27** were made in dimethylsulfoxide (Fluka Chemie AG Buchs, Switzerland) at a concentration of 10 mM, filtered through Millipore filter (0.22 μM), before use, and afterwards diluted to various working concentrations with RPMI-1640 nutrient medium (Sigma Chemical Co. St Louis, MO) supplemented with 3 mmol/L L-glutamine, 100 μg/mL streptomycin, 100 IU/mL penicillin, 10% heat inactivated fetal bovine serum (FBS - Sigma Chemical Co.), and 25 mM Hepes, adjusted to pH 7.2 by bicarbonate solution.

4.2.1. Treatment of HeLa, LS174 and K562 cells

HeLa and LS174 cells were seeded into 96-well microtiter plates (2000 and 5000 cells, respectively, in 0.1 mL of nutrient medium per well); K562 cells were maintained as suspension culture. After 20 h, to wells with HeLa and LS174 cells, five different concentrations of **1**–**27** were applied, except to the control wells, the wells with cells grown in a nutrient medium only. To K562 cells (3000 cells per well), investigated compounds were added 2 h after the cell seeding. All concentrations were set up in triplicate. Nutrient medium with corresponding concentrations of investigated compounds, but without cells, was used as a blank, also in triplicate.

4.2.2. Determination of cell survival

HeLa, LS174 and K562 cell survival, was determined by MTT test, according to Mosmann [28], with modification by Ohno and Abe [29], 72 h upon addition of the compound. Briefly, 20 μL of MTT solution (5 mg/mL PBS) were added to each well. Samples were incubated for further 4 h at 37 °C in 5% CO_2 and humidified air atmosphere. Then, 100 μL of 10% SDS were added to the wells. Absorbance at 570 nm was measured the next day. To get cell survival (%), absorbance of a sample with cells grown in the presence of various concentration of **1**–**27** was divided by the control absorbance (the absorbance of sample with cells grown in nutrient medium only), and multiplied by 100. It was implied that absorbance of blank was always subtracted from absorbance of a corresponding sample with target cells. IC_{50} concentration was given as the concentration of agent that inhibits cell survival by 50%, compared with vehicle-treated control. All IC_{50}'s were reported as a mean of three measurements, each done in triplicate.

4.2.3. Cell cycle determination

Cell cycle determination was done on HeLa cells. Aliquots of 5×10^5 control cells, or cells treated with compound **19**, during 24 h, 48 h and 72 h (in concentration of two IC_{50} values, where IC_{50} was as obtained after 72 h of incubation with compound, as described above), were fixed in 70% ethanol on ice for the one week, and then centrifuged. The pellet was treated with RNase A (100 μg/mL) at 37 °C for 30 min, and then incubated with 40 μg/mL of propidium iodide (PI) for at least 30 min. Cells were analyzed using a FACSCalibur flow cytometer (BD Biosciences Franklin Lakes, NJ, USA), equipped with a 15 mW, air-cooled 488 nm argon ion laser for excitation of PI. The PI fluorescence (FL2) was collected after passing a 585/42-nm band pass filter. FACSCalibur flow cytometer equipped with an FL2 upgraded doublet discrimination module (DDM), allows screening, and then excluding possible occurrence of cell doublets, clumps and debris, by plotting FL2-area versus FL2-width signals [30]. PI fluorescence data was collected using linear amplification. For the each sample 20,000 events was collected. Finally, data were analyzed using CELLQuest 3.2.1.f1 software (BD Biosciences).

4.3. Modeling

For modeling purposes IC_{50}, in molar concentrations, were converted to corresponding negative decade logarithms, $p(IC_{50})$. The SMILES notation of **1**–**27** were converted to 3D by OMEGA [31], using MM94FF [32], and further optimized by MOPAC 2009 to root-mean square gradient of 0.001 kcal mol^{-1} A^{-1}, by semiempirical MO PM6 method [33], using implicit solvation in water (COSMO) [34]. During optimization constraint is imposed on ketovinyl moiety. VegaZZ [35] was used as GUI. All optimized structures were saved in mol2 format and submitted to Pentacle software for an alignment-free 3D QSAR analysis. Molecular interaction fields are computed using built-in GRID program [36], with grid resolution of 0.4 Å. AMANDA algorithm were used for extraction of hot spots (nodes) from obtained MIFs' (discretization); distances and relative position of nodes were described by CLAC algorithm (encoding), suitable for examination of the group of congeneric compounds. Five principal components/latent variables were initially used for both principal component analysis (PCA) and partial least square (PLS) model. Final PLS models were reported with three latent variables (LV) for the potency of compounds toward HeLa and LS174 cells, and with 4LV for potency of compounds toward K562 cells.

Compounds extracted from NCI-DTP database were saved in SMILES format (including stereochemistry assignation), converted to 3D by OMEGA, and optimized on semiempirical MO level, using same settings as for **1**–**27**. Database were built in Pentacle virtual screening mode (VS), using default settings: grid resolution 0.5 Å, DRY, O, N1 and TIP probes, AMANDA algorithm for extraction of the hot spots, and MACC algorithm for encoding.

The 3D dependent whole molecular properties, molecular surfaces (solvent accessible, polar, apolar), volume and virtual log*P* are calculated by VegaZZ 2.4.0 [35]. BICUBE [37] was used to extract isosurfaces from molecular interaction fields, obtained by GRID hydrophobic (DRY), hydrogen bond donor/hydrogen bond acceptor (OH2), and H probes. The last probe is used to characterize molecular shape, while DRY and OH2 probes are chosen to characterize hydrophobic and polar part of molecules, respectively. HOMO and LUMO energies were extracted from MOPAC output files, and orbitals are visualized by Jmol [38]. Multiple linear regression (MLR) analysis was performed by BILIN program [39]. All calculations were done on AMD dual core ×64 processor (5 GHz) in Windows or Linux environments.

4.3.1. GRIND methodology

Program Pentacle uses alignment independent descriptors derived from GRID molecular interaction fields (MIF). More negative value of GRID MIF for any used probe corresponds to

more favorable interaction between a probe (e.g. hydrogen bond donor, hydrogen bond acceptor, hydrophobic) and a molecule for which the GRID MIF is calculated. By calculating MIFs for different GRID probes around a molecule and extracting most relevant regions one can obtain a fingerprint of a receptor to which small molecule could fit well. These regions show favorable energy of interaction and represent positions where groups of a potential receptor would interact favorably with a ligand. Such MIF pattern can be described as the virtual receptor site (VRS). The each GRIND descriptor consists of two nodes extracted from MIFs and encodes their energy product and the spatial distance. GRIND variables represent geometrical relationships between relevant pharmacophoric points around studied molecules, which are entirely invariable to position of molecule(s) in space and alignment of molecules. Derivation of GRIND descriptors includes next steps: (i) computing a set of MIF around studied molecules, (ii) filtering the MIF, to extract the most relevant regions that define the VRS, and (iii) encoding the VRS into the GRIND variables. In our models the CLAC algorithm, suitable for examination of the set of congeneric compounds, is used. GRIND variables can be used for comparison of molecules and their classification within sets of structurally diverse entities, and Pentacle program use principal component analysis (PCA) for this type of analysis. A dependent variable (such is biological activity of a certain type) can be correlated to GRIND descriptors (as independent variables), obtained on a set of molecules, by partial least square analysis (PLS). Most intensive bars in the PLS plots have the highest impact on a model. Bars having positive values on *y* scale represent variables positively correlated with activity, while those having negative values on *y* scale are negatively correlated with activity. Within the each block (auto- or cross-correlograms, that correspond to pairs of nodes of a same or a different probe, respectively) variables are arranged from left to right on the *x* scale of the plot, according to ascending distance between their nodes. In addition to the spatial arrangement of molecules and nodes encoded in GRIND variables, each node of each variable exert specific energy of interaction with a target molecule. Therefore, the strength of interaction between respective GRID probe in particular node and molecules are accounted in addition to the spatial positions of VRS regions. Pentacle use GRIND-2, the second generation of GRID-based alignment independent descriptors. For more information see reference [18b] and http://cadd.imim.es/grib-cadd/projects/pentacle.

5. Contributions

B.J. Drakulić design, prepares, purify, characterize compounds, and done all modeling work. B.J. Drakulić write article from draft to the final version. T.P. Stanojković make biological tests (IC_{50} determination). Ž.S. Žižak make biological tests (IC_{50} and cell cycle determinations) and commented results of the effect of compound on cell cycle. M.M. Dabović insightfully commented final version. Authors declare no conflict of interest.

Acknowledgement

Ministry of Science and Technological Development of Serbia support this work. Grant 172035.

Appendix. Supplementary material

Supplementary data associated with this article can be found in the online version, at doi:10.1016/j.ejmech.2011.04.043.

References

[1] H. von Peschman, Ueber Condensationsprodukte zweibasischer Fettsäuren, Ber. Dtsch. Chem. Ges 15 (1882) 881–892.
[2] a) H. Rinderknecht, J.L. Ward, F. Bergel, A.L. Morrison, Studies on antibiotics. II. Bacteriological activity and possible mode of action of certain nonnitrogenous natural and synthetic antibiotics, Biochem. J. 41 (1947) 463–469;
b) B.J. Cramer, W. Schroeder, W.J. Moran, C.H. Nield, M. Edwards, C.I. Jarowski, B. Puetzer, The antibacterial activity of some β-aroyl-acrylic acids, esters, and amides, J. Am. Pharm. Assoc. Sci. 37 (1948) 439–449;
c) F.K. Kirchner, J.H. Bailey, C.J. Cavallito, Ring substituted benzoylacrylic acids as antibacterial agents, J. Amer. Chem. Soc. 71 (1949) 1210–1213;
d) N.H. Cromwell, P.L. Creger, K.E. Cook, Studies with the amine adducts of β-benzoylacrylic acid and its methyl ester, J. Amer. Chem. Soc. 78 (1956) 4412–4416;
e) A. Dal Pozzo, M. Acquasaliante, G. Donezzeli, P. De Maria, C. Nicoli, 3-Carbonylacrylic derivatives as potential antimicrobial agents. Correlations between activity and reactivity toward cysteine, J. Med. Chem. 30 (1987) 1674–1677;
f) K. Bowden, M.S. Dixon, J.R. Runson, Structure-activity relations. Part 4. Reactivity and anti-bacterial activity of 3-aroylacrylic acids and their methyl esters, J. Chem. Res. Synopses (1979) 8;
g) K. Bowden, A. Dal Pozzo, C.K. Duah, Structure-activity relations. Part 5. Antibacterial activity of a series of substituted (*E*)-3-(4-phenylbenzoyl)acrylic acids, -chalcones, -2-hydroxychalcones and -α-bromochalcones; addition of cysteine to substituted 3-benzoylacrylic acids and related compounds, J. Chem. Res. Synopses (1990) 2801–2830;
h) K. Bowden, M.P. Henry, Structure-activity relations. II. Antibacterial activity of 3-benzoylacrylic acids and esters, ACS Advances in Chemistry Series, Biol. Correl.-Hansch Approach, Symp. 114 (1972) 130–140.
[3] a) B.M. Anderson, M.L. Tanhcoo, A. Dal Pozzo, Selective enzyme inactivation by benzoylacrylic acid derivatives, Biochem. Biophys. Acta 703 (1982) 204–211;
b) B.M. Anderson, C.D. Anderson, G. Donzzeli, A. Dal Pozzo, Sulfhydryl enzyme inactivation by nicotinoylacrylates, Biochem. Biophys. Acta 787 (1984) 215–220.
[4] a) O. Dvorak, J. Venta, M. Semonsky, Report on treatment of advanced carcinoma of genitals with the preparation mbba, Neoplasma 12 (1965) 93–100;
b) O. Dvorak, Cytembena treatment of advanced gynaecological carcinomas, Neoplasma 18 (1971) 461–464;
c) O. Dvorak, J. Bauer, Cytembena treatment of advances and relapsing uterine cervix carcinoma, Neoplasma 18 (1971) 465–466;
d) Z. Matejovsky, Effects of Cytembena in the treatment of malignant musculoskeletal tumours, Neoplasma 18 (1971) 473–480.
[5] Z. Juranić, Lj. Stević, B. Drakulić, T. Stanojković, S. Radulović, I. Juranić, Substituted (*E*)-β-(benzoyl)acrylic acids suppressed survival of neoplastic human HeLa cells, J. Serb. Chem. Soc. 64 (1999) 505–512.
[6] S. Amslinger, The tunable functionality of α,β-unsaturated carbonyl compounds enables their differential application in biological systems, ChemMedChem 5 (2010) 351–356.
[7] D.L. Buckley, T.W. Corson, N. Aberle, C.M. Crews, Hiv Protease-mediated activation of sterically capped proteasome inhibitors and substrates, J. Am. Chem. Soc. 133 (2011) 698–700.
[8] a) S.K. Rabindran, C.M. Discafani, E.C. Rosfjord, M. Baxter, M.B. Floyd, J. Golas, W.A. Hallett, B.D. Johnson, R. Nilakantan, E. Overbeek, M.F. Reich, R. Shen, X. Shi, H.-R. Tsou, Y.-F. Wang, A. Wissner, Antitumor Activity of HKI-272, an orally active, irreversible inhibitor of the HER-2 tyrosine kinase, Cancer Res. 64 (2004) 3958–3965;
b) L.V. Sequist, B. Besse, T.J. Lynch, V.A. Miller, K.K. Wong, B. Gitlitz, K. Eaton, C. Zacharchuk, A. Freyman, C. Powell, R. Ananthakrishnan, S. Quinn, J.-C. Soria, Neratinib, an irreversible pan-ErbB receptor tyrosine kinase inhibitor: results of a phase II trial in patients with advanced non-small-cell lung cancer, J. Clin. Oncol. 28 (2010) 3076–3083.
[9] A. Wissner, E. Overbeek, M.F. Reich, M.B. Floyd, B.D. Johnson, N. Mamuya, E.C. Rosfjord, C. Discafani, R. Davis, X. Shi, S.K. Rabindran, B.C. Gruber, F. Ye, W.A. Hallett, R. Nilakantan, R. Shen, Y.-F. Wang, L.M. Greenberger, H.-R. Tsou, Synthesis and structure-activity relationships of 6,7-disubstituted 4-anilinoquinoline-3-carbonitriles. The design of an orally active, irreversible inhibitor of the tyrosine kinase activity of the epidermal growth factor receptor (EGFR) and the human epidermal growth factor receptor-2 (HER-2), J. Med. Chem. 46 (2003) 49–63.
[10] D.G. Covell, A. Wallqvist, R. Huang, N. Thanki, A.A. Rabow, X-Jun Lu, Analysis of gene expression, small-molecule screening and structural databases, Proteins 59 (2005) 403–433.
[11] R.H. Shoemaker, The NCI60 human tumour cell line anticancer drug screen, Nat. Rev. Cancer 6 (2006) 813–823.
[12] a) A.-M. Katsori, D. Hadjipavlou-Litina, Chalcones in cancer: understanding their role in terms of QSAR, Curr. Med. Chem. 16 (2009) 1062–1081;
b) J.R. Dimmock, G.A. Zello, E.O. Oloo, J.W. Quail, H.-B. Kraatz, P. Perjesi, F. Aradi, K. Takacs-Novak, T.M. Allen, C.L. Santos, J. Balzarini, E. De Clercq, J.P. Stables, Correlations between cytotoxicity and topography of some 2-arylidenebenzocycloalkanones determined by X-ray crystallography, J. Med. Chem. 45 (2002) 3103–3111.
[13] B.J. Drakulić, G.A. Bogdanović, S.B. Novaković, I.O. Juranić, Crystal structure of (*E*)-4-phenyl-4-oxo-2-butenoic acid, 41st Conference of the Serbian Chemical Society, Book of Abstracts, p. 191, Belgrade 2003.

[14] S.B. Novaković, G.A. Bogdanović, B.J. Drakulić, A. Spasojević-de Biré, I.O. Juranić, Electronic and topological properties of the non-covalent interactions in derivative of benzoylacrylic acid, Second Humboldt Conference on Non-covalent Interactions, Book of abstracts, p. 45, Vršac, Serbia, 2009. Full article in preparation.
[15] a) N. Sugiyama, H. Kataoka, C. Kashima, K. Yamada, The photoreaction of β-benoylacrylic acid, Bull. Chem. Soc. Jpn. 42 (1969) 1353–1356;
b) B.J. Drakulić, Synthesis, Epoxidation and Photoisomerization of Ar-aroylacrylic Acids, Graduate thesis, Faculty of Chemistry, University of Belgrade, February 1996, Belgrade.
[16] H.N. Patia, U. Dasa, R.K. Sharmab, J.R. Dimmock, Cytotoxic thiol alkylators, Mini-Rev. Med. Chem. 7 (2007) 131–139.
[17] F. Fontaine, M. Pastor, F. Sanz, Incorporating molecular shape into the alignment-free GRid-INdependent descriptors, J. Med. Chem. 47 (2004) 2805–2815.
[18] a) M. Pastor, G. Cruciani, I. McLay, S. Pickett, S. Clementi, GRid-INdependent descriptors (GRIND): a novel class of alignment-independent three-dimensional molecular descriptors, J. Med.Chem. 43 (2000) 3233–3243;
b) A. Durán, G. Comesaña, M. Pastor, Development and validation of AMANDA, a new algorithm for selecting highly relevant regions in molecular interaction fields, J. Chem. Inf. Mod. 48 (2008) 1813–1823.
[19] Pentacle v. 1.0.5, Molecular Discovery Ltd, http://www.moldiscovery.com (accessed on 03.04.11).
[20] P. Gaillard, P.A. Carrupt, B. Testa, A. Boudon, Molecular lipophilicity potential, a tool in 3D QSAR: method and applications, J. Comput. Aid. Mol. Des 8 (1994) 83–96.
[21] a) B.J. Drakulić, Z.D. Juranić, T.P. Stanojković, I.O. Juranić, 2-[(Carboxymethyl) sulfanyl]-4-oxo-4-arylbutanoic acids selectively suppressed proliferation of neoplastic human HeLa cells. A SAR/QSAR study, J. Med. Chem. 48 (2005) 5600–5603;
b) M.D. Vitorović-Todorović, I.O. Juranić, L.M. Mandić, B.J. Drakulić, 4-Aryl-4-oxo-*N*-phenyl-2-aminylbutyramides as acetyl- and butyrylcholinesterase inhibitors. Preparation, anticholinesterase activity, docking study, and 3D structure–activity relationship based on molecular interaction fields, Bioorg. Med. Chem. 18 (2010) 1181–1193;
c) B.J. Drakulić, unpublised results;
d) B.J. Drakulić, M.D. Vitorović-Todorović, I.N. Cvijetić, unpublised results.
[22] A.T. Dinkova-Kostova, M.A. Massiah, R.E. Bozak, R.J. Hicks, P. Talalay, Potency of Michael reaction acceptors as inducers of enzymes that protect against carcinogenesis depends on their reactivity with sulfhydryl groups, Proc. Natl. Acad. Sci. USA 98 (2001) 3404–3409.
[23] A. Duran, I. Zamora, M. Pastor, Suitability of GRIND-Based principal properties for the description of molecular similarity and ligand-based virtual screening, J. Chem. Inf. Model. 49 (2009) 2129–2138.
[24] W.J. Houlihan, J. Nadelson, for Sandoz Inc. patent, US 4083997, 1978.
[25] D. Papa, E. Schwenk, F. Villani, E. Klingsberg, β-Aroylacrylic acids, J. Am. Chem. Soc. 70 (1948) 3356–3360.
[26] Haung-Minlon, A simple modification of the Wolff-Kishner reduction, J. Am. Chem. Soc. 68 (1946) 2487–2488.
[27] N.J. Kim, K.H. Chung, E.K. Ryu, Friedel-Crafts cyclohexylation of arenes with 1,3-dicyclohexylcarbodiimide (DCC), Tetrahedron Lett. 35 (1994) 903–904.
[28] T. Mosmann, Rapid colorimetric assay for cellular growth and survival: application to proliferation and cytotoxicity assays, J. Immunol. Methods 65 (1983) 55–63.
[29] M. Ohno, T. Abe, Rapid colorimetric assay for the quantification of leukemia inhibitory factor (LIF) and interleukin-6 (IL-6), J. Immunol. Methods 145 (1991) 199–203.
[30] M. Carbonari, T. Tedesco, M. Fiorilli, A unified procedure for conservative (morphology) and integral (DNA and immunophenotype) cell staining for flow cytometry, Cytometry 44 (2001) 120–125.
[31] J. Boström, Reproducing the conformations of protein-bound ligands: a critical evaluation of several popular conformational searching tools, J. Comput. Aid. Mol. Des. 15 (2001) 1137–1152.
[32] T.A. Halgren, Merck molecular force field. I. Basis, Form, Scope, Parameterization, performance MMFF94, J. Comput. Chem. 17 (1996) 490–519.
[33] J.J.P. Stewart, Optimization of parameters for semiempirical methods V: modification of NDDO approximations and application to 70 elements, J. Mol. Mod. 13 (2007) 1173–1213.
[34] A. Klamt, G. Schüümann, COSMO: a new approach to dielectric screening in solvents with explicit expressions for the screening energy and its gradient, J. Chem. Soc. Perkin Trans. 2 (1993) 799–805.
[35] A. Pedretti, L. Villa, G. Vistoli, VEGA - An open platform to develop chemo-bio-informatics applications, using plug-in architecture and script programming, J. Comput. Aid. Mol. Des 18 (2004) 167–173. http://www.ddl.unimi.it VegaZZ 2.4.0 (accessed on 03.04.11).
[36] a) P.J. Goodford, A computational procedure for determining energetically favorable binding sites on biologically important macromolecules, J. Med. Chem. 28 (1985) 849–857. http://www.moldiscovery.com GRID v.22b Molecular Discovery Ltd. (assessed on 03.04.11);
b) G. Cruciani (Ed.), Molecular Interaction Fields. Applications in Drug Discovery and ADME Prediction, Wiley-VCH, Zurich, Switzerland, 2006.
[37] G. Caron, A. Nurisso, G. Ermondi, How to extend the use of grid-based interaction energy maps from chemistry to biotopics, ChemMedChem 4 (2009) 29–36. www.casmedchem.unito.it (assessed on 03.04.11).
[38] Jmol v11.2.10, an open-source Java viewer for chemical structures in 3D. http://www.jmol.org/ (assessed on 03.04.11).
[39] H. Kubinyi, Non-linear dependence of biological activity on hydrophobic character: the bilinear model, J. Med. Chem. 20 (1977) 625–629. http://www.kubinyi.de/bilin-program.html (assessed on 03.04.11).